3

Positron Source

Contents

3.1 Introduction . . . 81
3.1.1 Overview . . . 81
3.1.2 System Description . . . 81
3.1.3 Parameters . . . 82
3.2 Positron Yield Simulation . . . 82
3.2.1 Target Yield . . . 86
3.2.2 Ray Tracing through Capture Accelerator . . . 86
3.3 Drive Electron Accelerator . . . 86
3.3.1 Drive Electron Source . . . 86
3.3.2 Drive Linac . . . 88
3.4 Positron Production Target . . . 88
3.4.1 Review of Target Test Data . . . 88
3.4.2 Electron Beam Size . . . 89
3.4.3 Beam Power and Target Size . . . 89
3.4.4 Target Engineering Issues . . . 89
3.4.5 Backup Power . . . 92
3.4.6 Integration with Positron Collection System . . . 93
3.5 Positron Collection System . . . 93
3.5.1 Flux Concentrator . . . 93
3.5.2 High Gradient L-Band Capture Accelerator . . . 93
3.5.3 Tapered-Field and Uniform-Field Solenoids . . . 94
3.5.4 Space Charge . . . 94
3.6 Beam Dynamics and Transport . . . 94
3.6.1 Control of Multibunch Beam Blow-up in Positron Linac . . . 94
3.6.2 Aperture and Beam Optics System Parameter . . . 95
3.6.3 Beam Position and Emittance Control . . . 96
3.7 Positron Linac . . . 98
3.8 Radiation Control Issues . . . 98
3.8.1 Design Plan for Maintenance . . . 98
3.8.2 Radiation Shielding . . . 98
3.8.3 Radiation Hard Components . . . 99
3.9 Magnets . . . 101
3.9.1 Solenoids . . . 101
3.9.2 Quadrupoles . . . 101
3.9.3 Bending Dipoles . . . 101
3.10 Diagnostics and Instrumentation . . . 101

3.10.1 Specifications . . . 102
3.10.2 Beam Intensity . . . 102
3.10.3 Beam Position . . . 102
3.10.4 Beam Size . . . 103
3.10.5 Beam Bunch Length . . . 103
3.10.6 Energy . . . 103
3.10.7 Energy Spread . . . 103
3.10.8 RF Phase and Amplitude Monitoring . . . 104
3.11 Feedback and Stability . . . 104
3.11.1 Intensity Uniformity Specifications . . . 104
3.11.2 Transverse Orbit Stability . . . 104
3.11.3 Energy Control . . . 105
3.12 Operations and Tuning Procedures . . . 105
3.13 Control System Needs . . . 105
3.13.1 Specification . . . 105
3.13.2 Special Requirements . . . 105
3.14 Other Considerations . . . 106
3.15 Summary . . . 106

3.1 Introduction

3.1.1 Overview

The baseline positron source for the NLC is a conventional source based on an electromagnetic shower created by high-energy electrons impinging on a thick, high-Z target. Its design draws heavily on that of the SLC positron source, which has demonstrated excellent reliability over many years of operation. The source and its associated 2-GeV linac, initially built for the 500-GeV center-of-mass machine (NLC-I), must be upgradeable by simply doubling the energy of the incident electrons to produce the charge per pulse that meets the specification of the 1-TeV center-of-mass machine (NLC-II). In particular, NLC-II requires a train of 90 bunches with up to 1.25×10^{10} positrons/bunch in each accelerator pulse, at a pulse repetition rate of 120 Hz. This is a charge per pulse of about 23 times the design intensity of the SLC positron source. Target tests performed during the SLC R&D indicated a small (about 40%) margin of safety between the design and the destruction of the target from pulse heating. It appears wise to keep the pulse energy deposition density in the target below the SLC design value. Thus, the positron beam pulse intensity may be increased only by increasing the size of the drive electron beam to allow for increased pulse energy deposition in the target and by increasing the admittance of the positron capture system.

Therefore, the following strategy has been adopted in designing the positron source for NLC-II: (1) double the radius of the incident electron beam which allows the pulse energy deposition in the target, and hence the pulse positron production, to be quadrupled; (2) accelerate the positrons at an L-band frequency of 1428 MHz in a structure with an aperture slightly more than twice larger than the SLC source while maintaining the magnetic field of the uniform-field solenoid at the same value as in the SLC source. Doubling the beam radius on the target roughly quadruples the 4-D emittance of the outgoing positrons. However, the use of an L-band accelerator not only increases the 4-D transverse admittance by a factor of 16 but also doubles the longitudinal phase space admittance, though the benefit of the latter is not fully realized due to increased debunching caused by the more divergent particles. As a result, we find that the positron yield per electron per GeV is more than quadrupled in comparison with the SLC source. For NLC-I, a 50% increase in the radius of the incident electron beam is adequate. This leads to an improvement in the positron yield per electron per GeV by almost 40% over that of NLC-II. The net result of these scalings is that with incident electrons at 3.11 GeV and 6.22 GeV for NLC-I and NLC-II, respectively, the NLC source produces a positron beam with more than twice the intensity required at the interaction point. Such a safety margin is necessary for a conservatively designed positron source, as large beam losses may occur in transport through the booster linac and through the two damping rings. Assuming losses of 20% each in the booster linac and in the two damping rings and an additional 5% loss in the main linac and the final focus system, the source still boasts a 50% margin in beam intensity.

With the proposed scaling, the density of the energy deposited in the target for both machines is slightly below the SLC design, whereas the average deposited power is about a factor of 2.5 greater for both NLC-I and NLC-II. The higher average power is not a major problem, but it does exacerbate the problem of radioactivity which also has significant bearings on source maintainability. It will necessitate a larger-diameter rotating or trolling target and larger cooling water flow.

3.1.2 System Description

The proposed NLC positron source shares in design substantial similarity to its SLC counterpart. The conventional technique of producing positrons from $e^{\pm}$ pair production by bombarding a conversion target with high-energy electrons will be used. Three subsystems comprise the NLC positron source: an accelerator for the drive electron

beam, a positron production and collection system, and a positron booster linac. Figures 3-1 and 3-2 show a schematic layout of the NLC positron source. A brief description of each subsystem follows.

A DC electron gun, coupled to two subharmonic bunchers and an S-band buncher, produces an electron beam of the desired NLC multibunch structure, *i.e.,* with an inter-bunch spacing at 1.4 ns and a total of 90 bunches/pulse. The electron beam is then accelerated in an S-band linac to 3.11 GeV for the 500-GeV machine or 6.22 GeV for the 1-TeV upgrade before impinging on a positron production target. The drive beam intensity at the target is 1.5×10^{10} electrons/bunch.

The positrons emerging from the production target as a result of the electromagnetic shower cascade are captured by a 240-MeV L-band capture accelerator embedded in a uniform solenoidal field following an adiabatic phase-space matching device consisting of a flux concentrator and a tapered-field solenoid. The longitudinally varying magnetic field from the adiabatic matching device transforms the transverse phase space of the positron beam along the axis in such a way that

$$Br^2 = \text{const}, \tag{3.1}$$

and

$$B/p_\perp^2 = \text{const}, \tag{3.2}$$

where B is the magnetic field, r is the radial displacement, and $p_\perp$ is the transverse momentum. The choice for an L-band capture accelerator aims to boost mainly the 4-D transverse phase space acceptance by about a factor of 16 and the longitudinal phase space acceptance as well over a similarly designed S-band capture accelerator. The design employs a parallel dual source configuration for improved reliability. Electrons are dumped after the first bending magnet. Beam scrapers installed in between the bending doublet is used to to collimate the positron beam in energy as well as in transverse phase space prior to its injection into the booster linac.

The collimated positron beam, with the same bunch structure as the electron drive beam, is accelerated in an L-band booster linac to 2 GeV for emittance damping in a pre-damping ring followed by a main damping ring. The optics for the positron booster linac is a FODO array with its beta function scaled as E, which must suppress multibunch beam blow-up due to wakefields and limit chromaticity induced emittance growth. A large number of large-aperture quadrupole magnets surrounding the L-band accelerating sections and smaller-aperture quadrupole magnets elsewhere are used to form the lattice.

3.1.3 Parameters

The important parameters of the NLC positron source for both the 500-GeV and the 1-TeV machines are summarized in Table 3-1. The positron beam intensities are obtained from numerical simulation after optimizing various design parameters. As a reference, the operating and design parameters of the SLC positron source are also included.

3.2 Positron Yield Simulation

Positron yield simulations have been performed for both drive beam energies, *i.e.,* 3.11 and 6.22 GeV for NLC-I and NLC-II, respectively. The results are already presented in Table 3-1. In this section we shall discuss in detail the simulation results using a 6.22-GeV drive beam.

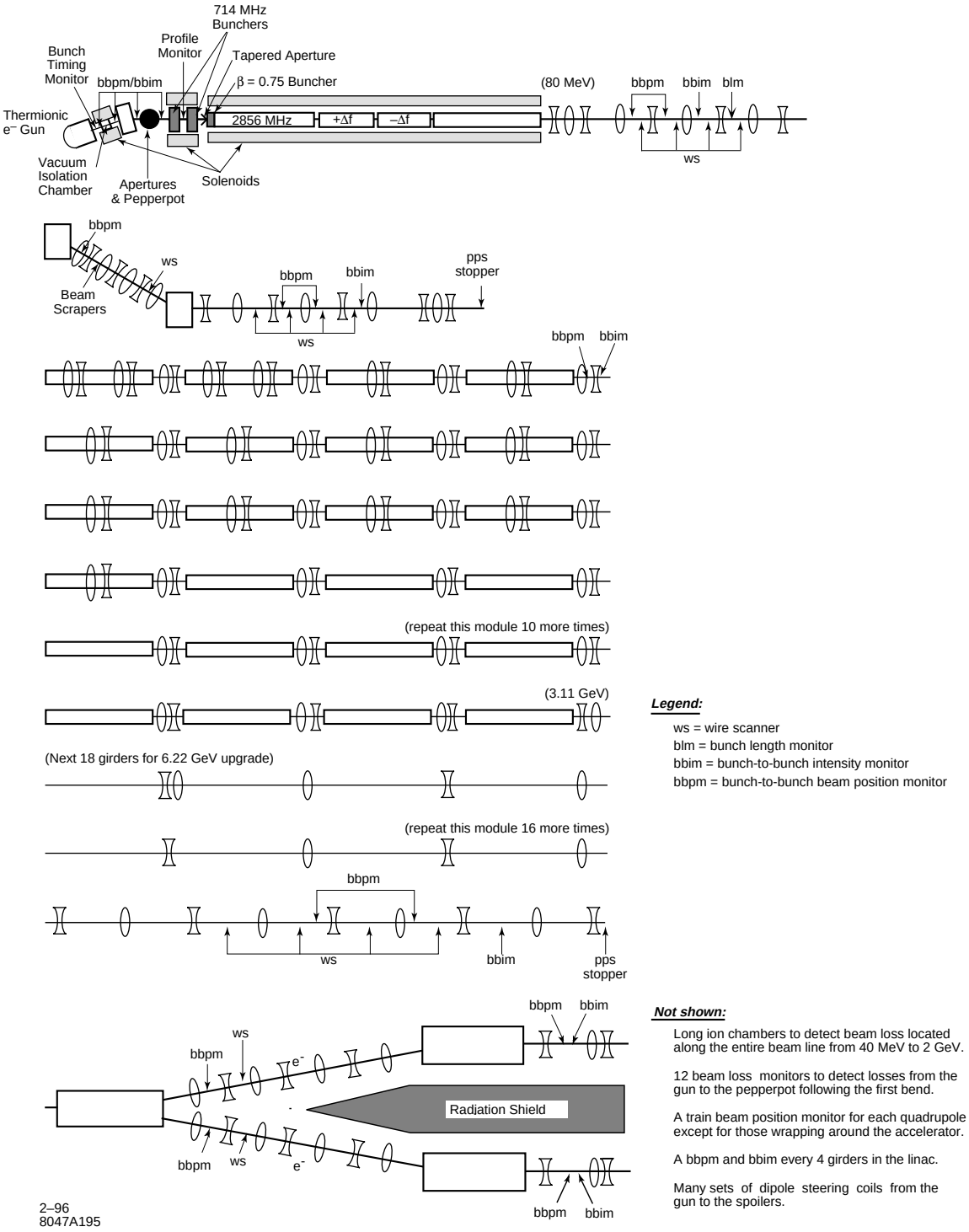

Figure 3-1. *Schematic layout of the NLC positron source (Part A): drive electron accelerator.*

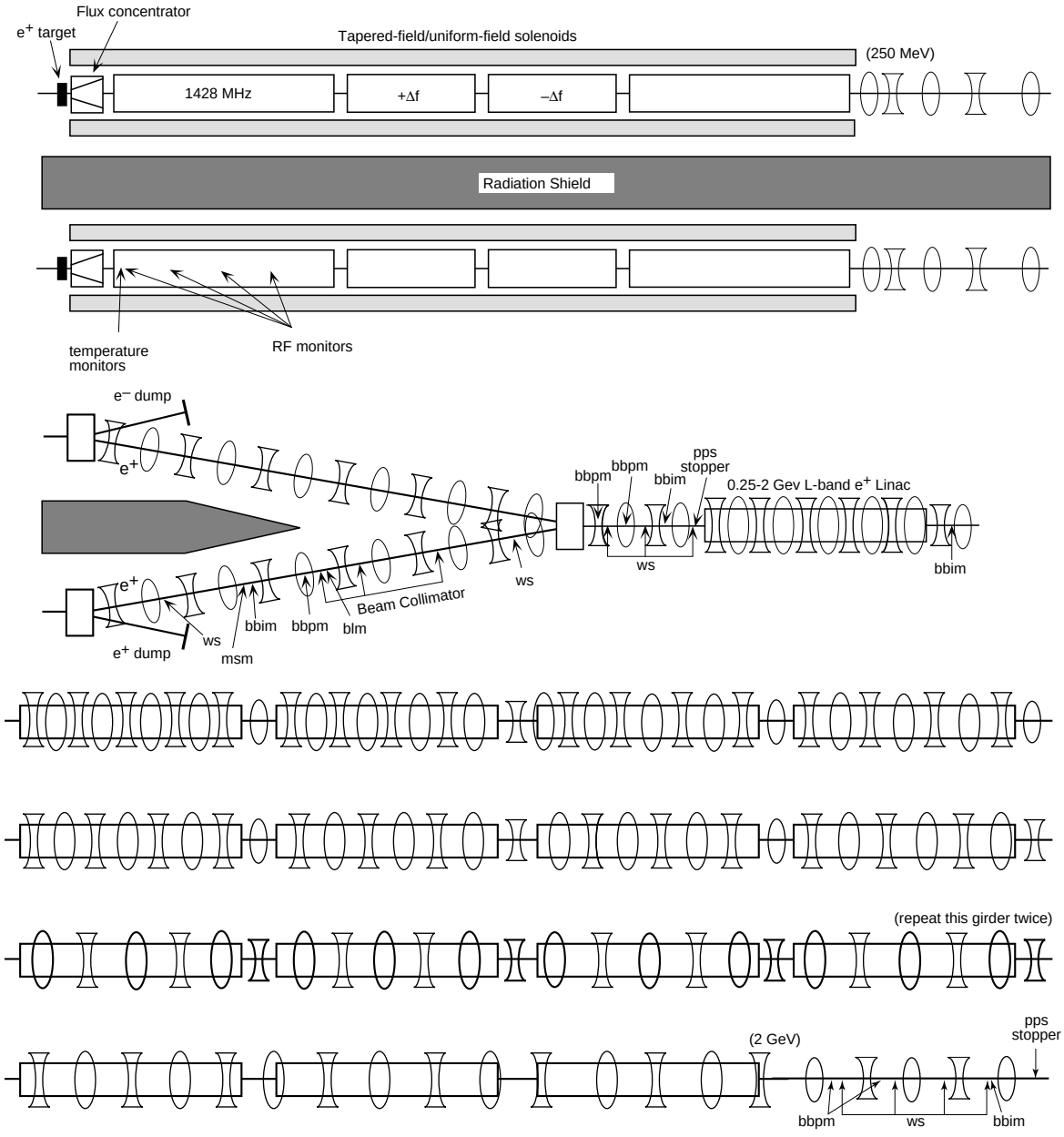

Legend:

ws = wire scanner
msm = multistrip monitor
blm = bunch length monitor
bbim = bunch-to-bunch intensity monitor
bbpm = bunch-to-bunch beam position monitor

Not shown:

Long ion chambers to detect beam loss located along the entire beam line from 250 MeV on up in energy.

Beam position monitors at each quadrupole except those wrapping around the accelerator.

Dipole steering coils strategically placed along the L-band linac from 250 MeV on.

4–96
8047A196

Figure 3-2. *Schematic layout of the NLC positron source (part B): dual positron production/capture systems and 1.75-GeV booster linac.*

Parameter	Unit	SLC 94	SLC max design	NLC-I (500 GeV)	NLC-II (1 TeV)
General Parameters:					
N_{e^+} per pulse at IP	$[10^{10}]$	3.5	5	76.5	112.5
# of bunches per pulse		1	1	90	90
Pulse duration	(ns)	0.003	0.003	126	126
Bunch spacing	(ns)	-	-	1.4	1.4
Repetition frequency	(hz)	120	180	180	120
Drive Electron Beam:					
Energy	(GeV)	30	30	3.11	6.22
N_{e^-} per bunch	(10^{10})	3.5	5	1.5	1.5
N_{e^-} per pulse	(10^{10})	3.5	5	135	135
Beam power	(kW)	20.2	47	121	161
RMS beam radius	(mm)	0.8	0.6	1.2	1.6
Beam energy density per pulse	(GeV/mm^2)	5.2×10^{11}	13.3×10^{11}	9.3×10^{11}	10.4×10^{11}
Positron Production Target:					
Material		$W_{75}R_{25}$	$W_{75}R_{25}$	$W_{75}R_{25}$	$W_{75}R_{25}$
Thickness	(R.L.)	6	6	4	4
Energy deposition per pulse	(J)	37	53	126	188
Power deposition	(kW)	4.4	9	23	23
Steady-state temperature	(°C)	100	200	400	400
Positron Collection:					
Accel. rf	(MHz)	2856	2856	1428	1428
Accel. gradient	(MV/m)	30	30	25	25
Minimum iris radius	(mm)	9	9	20	20
Edge emittance (allowing for 2 mm clearance)	(m-rad)	0.01	0.01	0.06	0.06
Positron yield per e^-		2.5[a]	2.5[a]	1.4	2.05
N_{e^+} per bunch	(10^{10})	8.7	12.5	2.1	3.1
N_{e^+} per pulse	(10^{10})	8.7	12.5	189	279

[a] The actual yield immediately following the capture section is 4, but decreases to 2.5 after two 180° bends and a 2-km transport line.

Table 3-1. *NLC Positron Source Parameters.*

3.2.1 Target Yield

The target yield for positrons has been calculated using the EGS program [Nelson 1985] for 6.22-GeV electrons impacting a $W_{75}Re_{25}$ target of thicknesses ranging from 4 to 6 radiation lengths. The optimal positron yield is obtained for a target thickness of about 5 radiation lengths. However, at this thickness about 23% of the beam energy is deposited in the target, as opposed to the 18% energy deposition in a 6-radiation-length-thick target in the SLC positron target. The increased volume density of energy deposition in the target is not desirable as it causes increased thermal stress which may lead to target failure. Therefore, a better choice would be to use a target of 4-radiation-lengths thick, for which the energy deposition is reduced significantly to about 14% while still retaining a respectable positron conversion yield. The total positron yield, defined as the number of positrons generated per incident drive electron, from such a target is about 12.5, whereas the total electron yield is about 15.8.

3.2.2 Ray Tracing through Capture Accelerator

The positron rays obtained from the EGS simulation have been traced through the flux concentrator and the capture accelerator up to the nominal 250-MeV point at the end of the capture region using the ETRANS program [Lynch 1989]. ETRANS is a ray tracing program developed at SLAC that integrates particle trajectories through static magnetic and rf fields while ignoring the effect of space charge and wakefields. The capture accelerator consists of two 5-m L-band (1428 MHz) accelerating sections with a loaded gradient of 25 MV/m and two off-frequency (1428 ± 1.4 MHz) 3-m sections for beam-loading compensation sandwiched in between the two accelerating sections. All four sections are embedded in a 0.5-T uniform solenoidal field. The rf phases of the accelerating fields in the capture region were varied to optimize the positron yield at the 250-MeV point. The best yield at the 250-MeV point, after applying energy and time cuts of ± 10 MeV and ± 30 ps, respectively, is found to be 2.05. With 1.5×10^{10} electrons/bunch in the drive beam, therefore, there will be approximately 3.1×10^{10} positrons/bunch in the L-band linac, which is a factor of 2.5 higher than the bunch intensity required at the interaction point. Figures 3-3 and 3-4 show the transverse and longitudinal phase space plots of the positron beam at the nominal 250-MeV point after the six-dimensional phase space cuts.

The electron rays emerging from the target were also traced through the capture accelerator. The electrons are approximately 65% more abundant than the positrons at the end of the capture system and have a most probable energy of about 230 MeV. These results are useful to evaluate the total beam loading in the capture accelerator and the power of the electron beam to be dumped after the first bending magnet.

3.3 Drive Electron Accelerator

3.3.1 Drive Electron Source

The baseline choice for the drive electron source is a DC thermionic cathode gun to be operated at 120 kV. A DC photocathode gun employing a bulk GaAs cathode and driven by a Ti:sapphire laser is considered as an option. The electron gun is required to deliver a very stable beam, with a pulse-to-pulse intensity jitter below 0.5% and a bunch-to-bunch intensity jitter below 2%. It is also required to have the capability to produce electron beams with variable bunch train structure to facilitate normal NLC operation as well as initial commissioning.

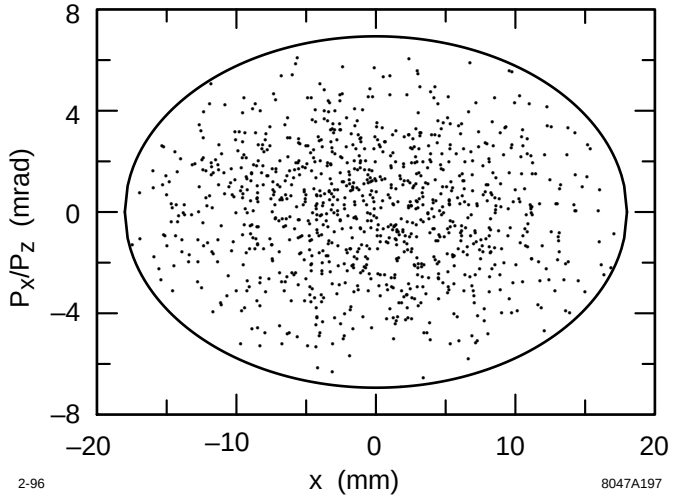

Figure 3-3. *Transverse phase space plot of the positron beam at the the exit of the capture accelerator.*

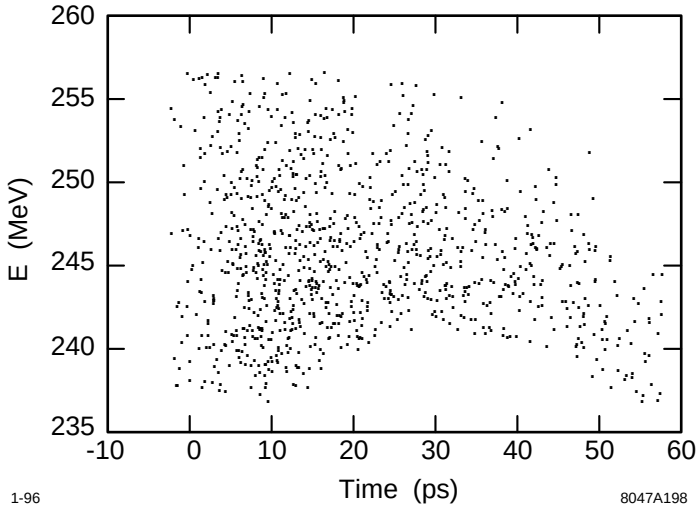

Figure 3-4. *Longitudinal phase space plot of the positron beam at the exit of the capture accelerator.*

The injector design for the drive electron beam is identical to that of the NLC electron source (see Chapter 2). To summarize briefly, it consists of two 714-MHz standing wave subharmonic bunchers and a 2856-MHz traveling wave ($\beta = 0.75$) S-band buncher, followed immediately by an 80-MeV S-band accelerator.

3.3.2 Drive Linac

The drive linac is also identical to the electron linac used in the NLC electron source except that it will be longer to accelerate the electrons to the higher energies required for efficient positron production. For NLC-I, the linac will end at 3.11 GeV, followed by a long drift section which will later be replaced by more accelerating sections to boost the energy to 6.22 GeV for the 1-TeV upgrade. Beam loading compensation in the linac will be accomplished by using the Δt approach. See Chapters 6 and 2 for details on the rf and lattice design issues.

3.4 Positron Production Target

The design of the NLC positron production target is modified significantly from that of the SLC target to accommodate the significantly higher beam power delivered to the NLC target. In addition, the target motion mechanism is modified from that of trolling as used in the SLC source to that of rotating to eliminate intensity modulations in the positron beam as experienced in the SLC. The periodic trolling motion of the target and its drive mechanism in the intense magnetic field of the tapered-field solenoid induces Eddy current in the moving parts. The Eddy current in turn generates a periodically varying magnetic field, leading to a small intensity modulation in the captured positron beam with the same frequency as that of the trolling motion. With a rotating target, however, the induced Eddy current should remain roughly constant, thus eliminating the source of intensity modulation.

3.4.1 Review of Target Test Data

Thermal stress from short pulse (or single pulse) heating is the underlying mechanism that causes material failure when a target is bombarded by a high-intensity, high-energy electron beam. As in the SLC positron source, $\mathrm{W_{75}Re_{25}}$ will be used as the target material for the NLC source because of its high-Z characteristic and its excellent thermal and mechanical properties. Material failure tests were conducted at SLAC in the early 1980s for W-Re targets with the Re concentration ranging from 18.6% to 27.6% [Ecklund 1981]. For these tests, the energy of the drive beam was in the range of 20–25 GeV, and the target thickness varied from 5–7 radiation lengths. The material failure threshold in terms of the maximum allowable beam energy density on the target per beam pulse was found to be approximately

$$\rho_{\max} = \frac{N\_E\_}{\pi\sigma^2} = 2 \times 10^{12}\,\mathrm{GeV/\,mm^2}\ , \tag{3.3}$$

with about 20% of the beam energy deposited in the target. In the above expression, $N\_$ is the number of electrons per pulse, $E\_$ the electron beam energy, and σ the rms radius of the electron beam on the target.

In the above, the failure threshold is expressed in an area beam energy density per pulse. While this is a convenient quantity to characterize the drive beam, it must be emphasized that the most critical parameter for causing material failure is the volume density of energy deposition per pulse in the target. However, the volume energy deposition density depends strongly on the longitudinal position across the target thickness, and it is the maximum density that matters the most for target failure considerations. In practice, it is also useful to evaluate the average energy deposition

density in the target. In terms of an average volume density, then, the failure threshold for $W_{75}Re_{25}$ is approximately 7×10^{10} GeV/ mm^2 per radiation length per pulse.

3.4.2 Electron Beam Size

For NLC-II, the drive beam has an energy of 6.22 GeV with a pulse intensity of $1.35 \times 10^{12} (= 90 \times 1.5 \times 10^{10})$ electrons. In order to avoid damaging the target, *i.e.,* to keep the energy density per beam pulse on the target comfortably below the threshold of 2×10^{12} GeV/ mm^2, the rms beam size of the incident electrons must be increased to 1.6 mm, twice the SLC drive beam size or four times the area. This yields a pulse beam energy density of 1.04×10^{12} GeV/ mm^2 on the target. For NLC-I, the beam radius may be reduced to 1.2 mm, yielding a pulse beam energy density on the target of about 0.93×10^{12} GeV/ mm^2. Since the electron beam size at the end of the 3.11-GeV or 6.22-GeV drive linac is typically much smaller than 1 mm (the normalized transverse emittance is less than 1×10^{-4} m·rad), a thin low-Z scatterer serving as an emittance spoiler must be used a few meters upstream of the target to blow up the beam size. For NLC-I and NLC-II, with 19% and 14% of the beam energy deposited in the 4-radiation-length thick target, the average volume density of energy deposition in the target is about 40% and 50% below the failure threshold, respectively.

3.4.3 Beam Power and Target Size

The average beam power deposited in the target amounts to approximately 23 kW for both NLC-I and NLC-II (Table 3-1). This power is about a factor of 2.5 and 5 larger than the SLC design and operating parameters, respectively. As the SLC positron production system has demonstrated good reliability, it is desirable to maintain a similar target size to beam power ratio for the NLC. Thus, by simply scaling the SLC target up a factor of 4, we find that the NLC target needs to have a diameter of about 20 cm. The target rotation frequency needs to be sufficiently high so that the areas of beam pulse impacts for two successive pulses do not overlap. Taking into account the increased beam size and the increased repetition rate (for NLC-I), the rotation frequency is chosen to be around 2 Hz.

3.4.4 Target Engineering Issues

By adopting a rotating target design, realizing a $\leq 1 \times 10^{-7}$-Torr vacuum in the target chamber in an environment of very high radiation levels becomes a challenging issue due to the lack of suitable materials for use as a leak-free seal around the rotating target shaft. Instead of pursuing a perfect vacuum seal, the present design seeks to achieve the vacuum goal by using a combination of conductance limiting seals and several stages of differential vacuum pumping.

Target Motion Mechanism, Monitoring and Control

The target wheel will be connected by way of a drive shaft and driven by an inline electric motor (Figure 3-5). The shaft will have two sets of outboard bearings such that the shaft is cantilevered into the target vacuum chamber. Similar to the SLC system, a stepping motor will be used to drive the target shaft, and an angular position sensor will be used for shaft angle and speed monitoring.

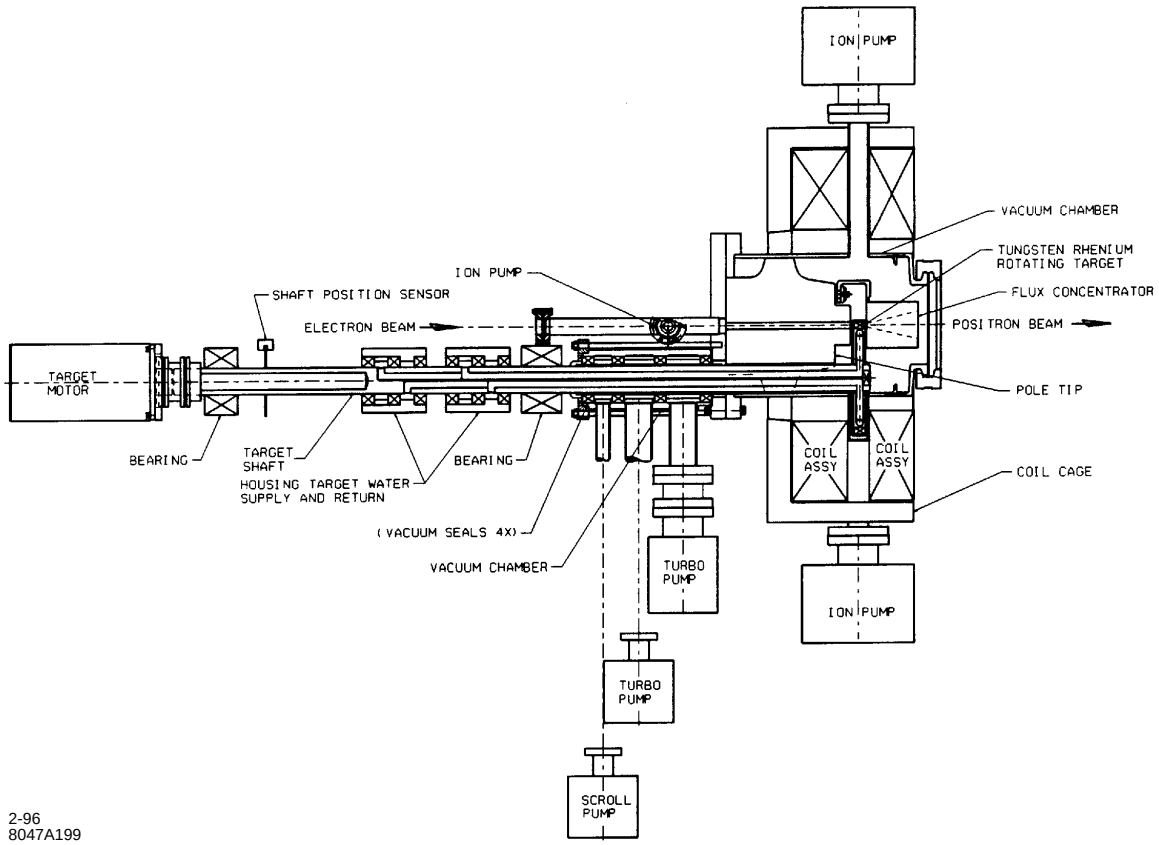

Figure 3-5. *Schematic of the NLC positron target system.*

Vacuum

The drive shaft will pass into the target vacuum chamber using a combination of radiation resistant seals and several stages of differential vacuum pumping along the length of the drive shaft (Figure 3-5). These seals involve a carbon and/or silver impregnated carbon element which rubs against a hard facing material such as tungsten carbide. These seals generally have tight clearances ($< 15\ \mu$m). Seal designs would be selected with leak path lengths of 25 mm or more. The leak rate goal for the first stage seal is on the order of 1 Torr-ℓ/s or less. Seals reviewed in the study included axial face seals, radial face seals, radial labyrinth seals, axial labyrinth seals, and magnetic face seals.

At least three stages and possibly four stages of differential vacuum pumping will be used along the drive shaft to isolate the rotating wheel target in the 1×10^{-7}-Torr vacuum from atmosphere. The first stage and possibly the second stage could use a dry scroll pump such as the Varian 600DS. This pump is completely oil free and has a base pressure in the 1×10^{-3}-Torr range. Differential pumping stages #2 and #3 or #3 and #4 (depending on the total number of stages used in the pumping system) could each use a turbomolecular pump such as the Varian Turbo-V70D. The Varian Turbo-V70D is a completely sealed, maintenance-free unit and is available in radiation-hardened configurations. The base pressure on these turbo pumps is 8×10^{-10} Torr. Each turbo pump will be backed with an oil free dry scroll pump. The vacuum objectives for the stages of differential pumping system in a three-stage system are: stage #1,

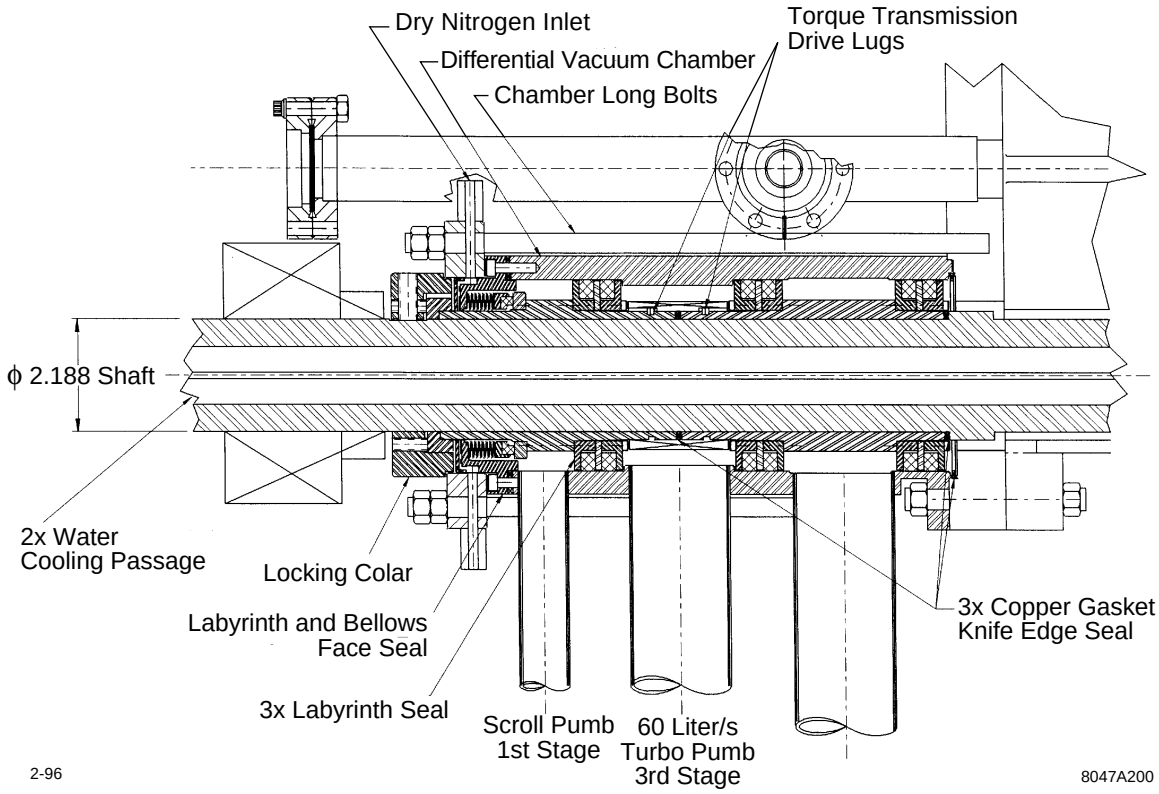

Figure 3-6. *NLC rotating target differential vacuum vacuum chamber and seals consept.*

1–3$\times 10^{-1}$ Torr; stage #2, 1–3$\times 10^{-4}$ Torr; stage #3, 1–3$\times 10^{-7}$ Torr. Vacuum in the target chamber will be about 1×10^{-7} Torr and provided by 30 ℓ/s or 60 ℓ/s ion pumps.

Figure 3-6 is a concept drawing showing a three-stage differential vacuum pumping system and support structure around the target drive shaft. This concept utilizes sets of radial labyrinth seals between vacuum pumping stages #1 and #2, stages #2 and #3, and again after stage #3. A bellows face seal with carbon contacting ring is used as the seal between atmosphere and stage #1.

A model two-stage differential pumping system with a rotating shaft will be built and experimented to prove the principle of this design and also to select the best seal materials.

Target Cooling

Figure 3-7 depicts a schematic cross-section view of the target wheel and drive shaft. Water supply and return lines will enter the shaft outside the vacuum space and pass through the center of the shaft to the target wheel assembly. The anticipated heat load on the wheel is about 23 kW for both NLC-I and NLC-II. The $W_{75}Re_{25}$ target element at the periphery of the wheel will be approximately 1.4-cm thick along the axial direction, and 1-cm thick in the radial direction. Cooling tubes will be located in a silver or copper casting adjacent to the $W_{75}Re_{25}$ target material to maximize the rates of heat conduction from the target to the cooling tube walls.

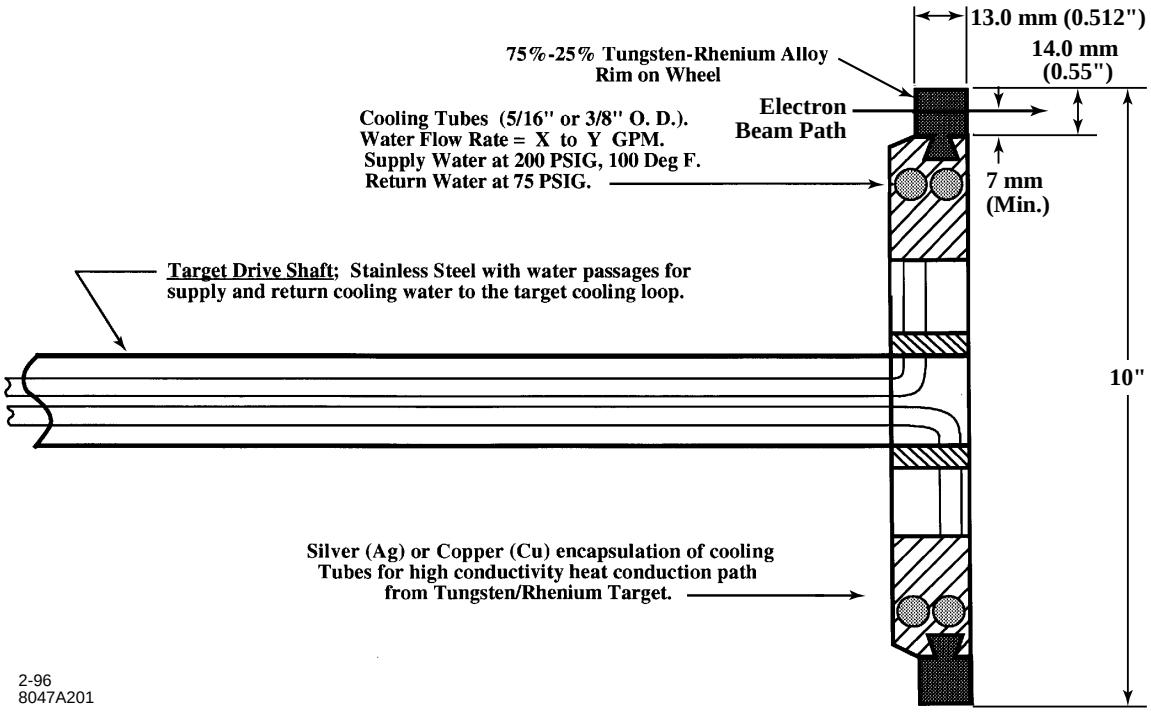

Figure 3-7. *NLC positron source target wheel schematic section.*

A high water velocity will be maintained in the cooling tubes (9–10 m/s) in order to yield a water side heat transfer film coefficient in the range of 17–20 kW/ m^2-°C. In order to produce the high cooling water velocity in the tubes, a water supply pressure of 200 psi (gauge) and return pressure of 75 psi (gauge) is assumed. Cooling water flow rate will be in a range of 80–120 ℓ/min by using cooling tubes with a 3/8-in or 5/16-in outer diameter.

For both NLC-I and NLC-II, temperature drops across the various components from the center of the beam impact point on the target to the cooling water are estimated to be as follows: ∼40°C across the water film inside the cooling tubes; ∼30°C across the stainless steel tubing wall; ∼50°C through the silver or copper casting around the cooling tubes from the $W_{75}Re_{25}$ target interface; and ∼220°C from the center of the beam impact point through the $W_{75}Re_{25}$ to the silver or copper interface. Thus, during operation, the maximum steady-state temperature in the target will be about 400°C which is quite comfortable for $W_{75}Re_{25}$. The steady-state temperature may be lowered substantially by modifications to the target design, such as reducing the radial thickness of the target to improve heat conductance.

The water supply and return lines to the target drive shaft will use radiation-hardened seals probably made from carbon and/or silver-filled carbon or metal composite.

3.4.5 Backup Power

The lack of a true vacuum seal in the positron target chamber means that, in the event of a power outage, the target chamber along with the capture accelerator will be vented due to lost pumping in the various stages. This will result in extended machine downtime as processing the accelerating sections following an air vent may take a long time.

Therefore, it is essential to have a reliable emergency backup power system. The backup system may include an uninterruptible power source as well as a power generator, both commercially available. In addition, the atmosphere side of the first stage seal will be flooded with dry N_2 gas. This is designed to provide further insurance that even in the event of a vent through the multi-stage seals the target chamber and the capture accelerator will be filled with dry N_2, which is relatively easy to pump out and processing the accelerator after venting to dry N_2 should be relatively quick. In addition, the use of a N_2 buffer gas also minimizes the amount of undesirable air gas species, such as H_2O, in the various differential pumping stages and the target chamber during normal operation.

3.4.6 Integration with Positron Collection System

The positron target system including its vacuum chamber must be closely mated to the flux concentrator and the subsequent capture accelerator to allow for efficient capture of positrons. As shown in Figure 3-5, the flux concentrator shares the same vacuum chamber as the target and is positioned close to it. The spacing between the flux concentrator and the first capture accelerating section must be kept at a minimum. Again, the SLC positron source serves as a design basis for these components and their integration.

3.5 Positron Collection System

The positrons emerging from the target have small spatial and temporal but large angular and energy distributions. Therefore, the use of a large-bandwidth phase-space transformer is essential to yield good capture efficiency of the positron beam into the capture accelerator which is embedded in a long solenoid magnet. As in the SLC positron source, a pulsed flux concentrator and a DC tapered-field solenoid [SLC 1984] will be used immediately following the conversion target to provide the adiabatically-varying longitudinal magnetic field which is essential for realizing the phase-space transformation [Helm 1962].

3.5.1 Flux Concentrator

The design and fabrication of the flux concentrator will follow exactly the SLC version [Kulikov 1991]. It is designed to produce a 5.8-T peak field along its axis. The minimum radius of the internal cone of the flux concentrator needs to be increased from 3.5 mm in the SLC version to 4.5 mm for the NLC to accommodate the increased radial extent of the emerging positron beam as a result of the increased incident electron beam size. The flux concentrator will be machined from a single block of Cu. The details of the fabrication process are described in the paper by Kulikov *et al.*, [Kulikov 1991]. The main advantage of using a flux concentrator is that it boosts the positron capture efficiency by a factor of 2–3 compared to a capture system utilizing a 1.2-T tapered field solenoid only.

3.5.2 High Gradient L-Band Capture Accelerator

For high capture efficiency, the positrons entering the capture accelerator must be accelerated to relativistic energies as quickly as possible to minimize bunch lengthening. Thus, the accelerating gradient needs to be as high as practically possible. The present design calls for the maximum unloaded gradient in the L-band capture accelerator, consisting of two 5-m accelerating sections and two 3-m beam loading compensation sections, to be 28 mV/m. To achieve

the desired gradient and also to facilitate beam loading compensation, each section will be powered by two 75-MW klystrons with SLED-I pulse compression. As the total beam loading current in the bunch train, including contributions from electrons as well as positrons both within and outside of the six-dimensional phase space acceptance window, can be up to 14 A for NLC-II, satisfactory beam loading compensation is realized only through the combined use of both Δt and Δf schemes. The positron beam energy at the end of the capture accelerator will be about 250 MeV, with a full energy spread of about $\pm 6\%$. The minimum iris radius of the disks will be 20 mm, and the outer radius of the disc-loaded waveguide will be about 11 cm. Chapter 6 contains more details on the rf design of the capture accelerator.

3.5.3 Tapered-Field and Uniform-Field Solenoids

A DC tapered-field solenoid producing a peak field of 1.2 T will be used in combination with the pulsed flux concentrator to serve as the phase space transformer, in which the magnetic field varies adiabatically from 7 T to 0.5 T. A 0.5-T uniform-field solenoid that encloses all four L-band accelerating sections will be used to provide transverse focusing in the capture accelerator. The design for the two solenoids is straightforward, as both have identical field specifications as those in the SLC positron source.

3.5.4 Space Charge

In this design, both the positrons and the electrons produced from the target will be collected and accelerated to about 250 and 230 MeV, respectively. The electrons will then be separated from the positrons after a bending magnet and dumped. In the region between the target and the accelerator, the electron bunch and the positron bunch overlap in space. Thus, wakefield and space charge forces will likely be insignificant. Once entering the capture accelerator, however, the positrons and the electrons will be quickly separated longitudinally, and space charge and wakefield forces may become important. However, experience from operating the SLC positron source suggests that the ETRANS simulation without taking into account space charge and wakefield forces is adequate.

3.6 Beam Dynamics and Transport

3.6.1 Control of Multibunch Beam Blow-up in Positron Linac

The normalized emittance of the bunches coming into the L-band linac just upstream of the positron pre-damping ring is $\gamma\varepsilon = 0.06\,\mathrm{m{\cdot}rad}$. The initial energy is 250 MeV and the final energy is that of the damping ring, 2 GeV. Other parameters of this linac assumed for the present simulations are shown in Table 3-2.

Calculations were performed using the program LINACBBU [Thompson 1990] which assumes smooth focusing scaling as an arbitrary power of energy. The effect of the focusing lattice was approximated by fitting an average beta function scaling as a power of energy. We obtained a beta function of 1.93 m at the beginning of the linac, and scaled it along the linac as $\beta = (E/E_i)\beta_i$. The resulting beam radius at the beginning of the linac is 1.8 cm. It will probably be desirable to strengthen the focusing at the beginning even more, to keep the beam size significantly smaller than the iris size.

Parameters	Values
Accelerating frequency	1428 MHz
Linac length	140 m
Initial energy	250 MeV
Final energy	2 GeV
Ne^+ per bunch	2.5×10^{10}
Bunch spacing	1.4 ns (2 rf buckets)
Initial beta function β_i (scales as E)	1.93 m
# bunches per train	90
Normalized emittance $\gamma\epsilon$	6×10^{-2} m·rad

Table 3-2. *Parameters of positron booster linac.*

The wake function was scaled from the SLC S-band linac, keeping the lowest 50 transverse dipole modes and assuming an uncoupled model. We examined the cases of: (1) a linear detuning with 4% total frequency spread; and (2) a Gaussian detuning of 10% total spread, where the truncation of the Gaussian distribution frequencies is at ± 2 sigma. There is about a maximum of 60% growth in the transverse offsets, for the case of a 4% linear spread. There is essentially no growth (approximately 4% maximum) in the transverse offsets, for the case of a 10% Gaussian detuning. In neither case did we include any damping beyond that of copper (we took the Qs of the modes to be 18400).

Effects of misalignments and frequency errors were not included in the results reported here, but we do not expect them to change our conclusion that the 10% Gaussian detuning should be fully adequate to control the multibunch emittance growth.

3.6.2 Aperture and Beam Optics System Parameter

The aperture of the positron linac is determined by the minimum aperture of the disk-loaded L-band accelerating structure, which will be 20 mm in radius. To allow for inevitable alignment and steering errors, the realistic transverse aperture for the beam is conservatively chosen to be 18 mm. This aperture, along with the 0.5-T longitudinal field for transverse focusing in the 240-MeV capture accelerator, defines the normalized edge emittance of the captured positron beam to be about 0.06 m·rad.

A preliminary beam optics design for transporting the 0.06-m· edge emittance positron beam through the two magnetic bends and in the common L-band linac to the positron pre-damping ring is shown in Figures 3-8 and 3-9. The design uses a scaled FODO lattice consisting of a dense array of quadrupole magnets. The quadrupole spacing is kept constant on the first accelerating section, and scaled as $\sqrt{E}$ on the remaining 23 sections. The quadrupole strengths are all kept nearly the same. The phase advance is 60° at the beginning of the lattice and gradually decreases along the linac. This design leads to a quasi-linear E scaling of the maximum beta function. The choice of relatively small phase advances is necessary to minimize the chromaticity-induced emittance growth, which has an initial full energy spread of $\pm 6\%$ at the 250-MeV point and decreases to about $\pm 2\%$ at the end of the L-band linac.

As shown in Figure 3-9, the full beam radius has shrunk to < 16 mm in the first 5-m section. From there on, the beam size is further reduced by the strong-focusing lattice to a final value of about 13 mm at the 2-GeV point. These results, obtained from first-order TRANSPORT runs, illustrate that the positron beam size can be controlled satisfactorily in the L-band linac. However, second-order TRANSPORT calculation shows that beam size control in the L-band linac is not as easy as the first order calculation indicates, mainly due to the inherent single-bunch energy spread of

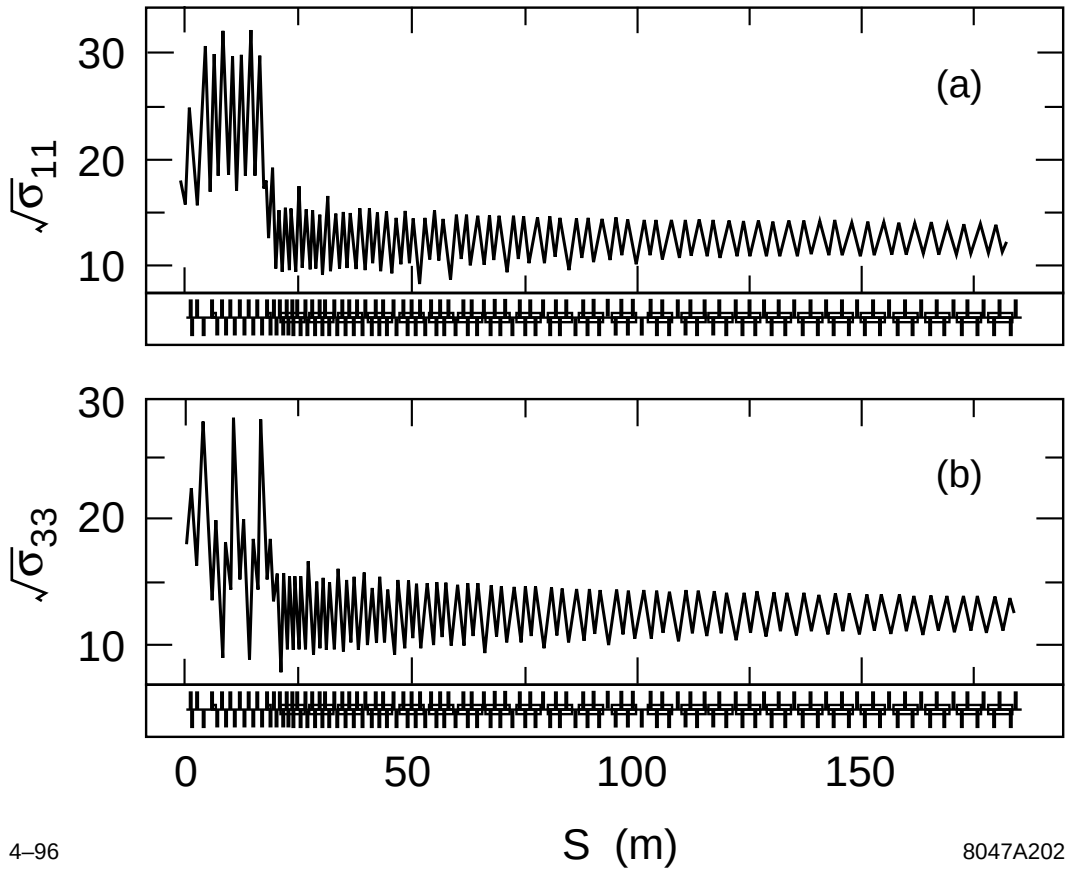

Figure 3-8. *Transverse size (edge radius) of the positron beam from the exit of the capture accelerator to the end of the L-band booster linac.*

the positron beam. This difficulty becomes more pronounced if the Δf beam-loading compensation scheme is used, which introduces large single-bunch energy spread along the linac. This is the main reason that the Δt scheme is chosen over the Δf scheme for beam loading compensation in the L-band positron linac.

3.6.3 Beam Position and Emittance Control

Due to the large transverse size of the positron beam and the limited aperture of the accelerating structure, reasonably good control (to within 0.2 mm) on the beam position is required throughout the 1.75-GeV L-band linac. A set of beam position monitors and X/Y steering correctors will be used to launch the positron beam into the linac. A beam position monitor and a pair of X/Y correctors will be installed in every gap between successive 5-m sections to maintain an optimal orbit in the L-band linac. It is also being considered to build beam position monitoring capabilities into the 5-m L-band structures by using the dipole signal so that the beam orbit in each 5-m section can be maintained at an optimum.

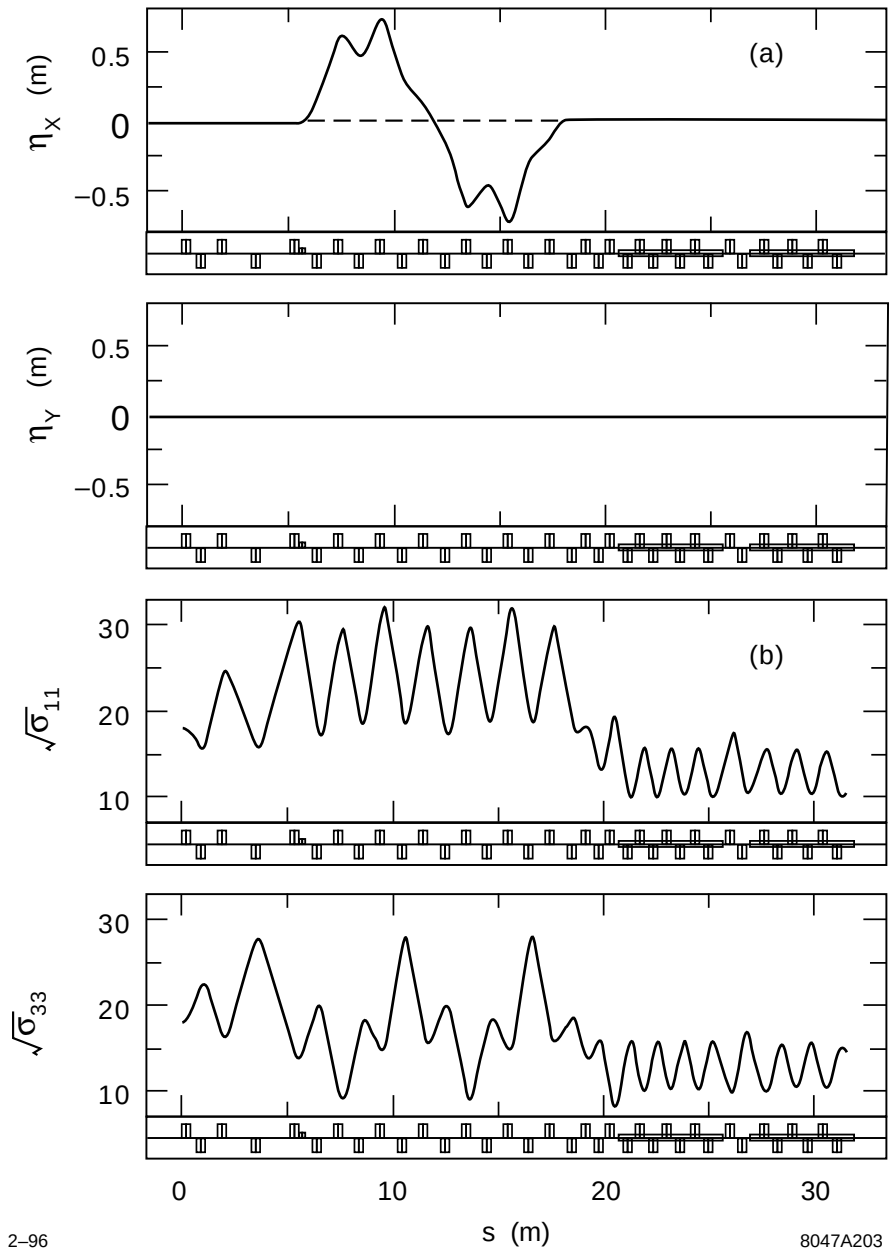

Figure 3-9. *Dispersion function and transverse beam size through the the double-bend achromat and in the first two 5-m L-band sections.*

Efficient injection into the pre-damping ring depends critically on the preservation of the beam emittance in the L-band linac. Emittance growth due to chromaticity, wakefields, beam line and magnets misalignment, etc., must be minimized.

3.7 Positron Linac

The L-band positron linac will consist of 12 accelerating modules. Each module contains two 5-m accelerating sections, which will be powered by two 75-MW L-band klystrons feeding a single SLED-I cavity. Beam loading compensation will be accomplished by using the Δt method, which offers the advantage of complete beam loading compensation at the end of each section without introducing single-bunch energy spread. The maximum attainable loaded energy gain for each module, assuming a beam current of 2.75 A across the bunch train, will be about 173 MeV. With an input beam energy of 250 MeV, the 12-module booster linac provides a large energy headroom—about 17% over the 2-GeV energy target.

3.8 Radiation Control Issues

3.8.1 Design Plan for Maintenance

Due to the high radiation activity in the areas around the target and the nominally 10-kW low-energy electron beam dump, access to these radiation-hot areas during a high-energy physics run must be delayed until the radiation activity drops to an acceptable level. As such cooling periods can be as long as several months, any maintenance work in these areas means extended downtime for the machine. A logical approach to improve the efficiency of the positron source is to add redundancy. In the present design, the positron source will have two identical positron vaults containing the positron production and collection systems, *i.e.*, from the target to the nominal 250-MeV point, adequately shielded from each other such that access to one vault is permitted while the other is in operation (Figure 3-10). The input electron beam can be directed to either system via a pair of bending dipoles which form an achromatic and isochronous beam line section. Likewise, the 250-MeV positron beam after the capture accelerator from either system can be directed into the 1.75-GeV L-band booster linac. If one system in use develops a problem during a run, we may quickly switch to the other system and continue the physics run. In the meantime, we can wait for the radiation level in the first positron vault to drop and then make an entry to repair or replace the broken components.

In addition to the dual positron vault design, efforts will be made to make the system components for positron production and collection as modular as possible to facilitate quick maintenance work. Use of materials that have long radiation decay times will be avoided.

3.8.2 Radiation Shielding

Primary Beam at Target

Figure 3-11 gives the calculated dose rate at 90° to a target-dump for various thicknesses of concrete shielding assuming a 150-kW beam of 6-GeV electrons impacting, conservatively chosen, a 30-cm-long and 10-cm-diameter

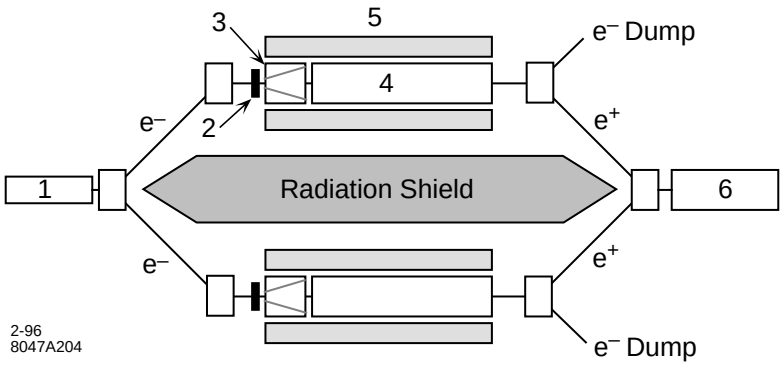

Figure 3-10. *An artist's view of the NLC positron source with two side-by-side positron production and capture systems: 1 – drive electron accelerator, 2 – positron target, 3 – flux concentrator, 4 – L-band capture accelerator, 5 – tapered-field and uniform-field solenoids, 6 – positron booster linac.*

iron target. The distance from the target to the shield is fixed at 1 m and the dose rate is determined at the outside surface of the shield. High-energy neutrons are the dominant component after about 2 m.

The integrated shield design limit is normally 500 mrem per year, which corresponds to 0.5 mrem/h for 1000 hours of operation in a year. This level, and the concrete thickness required to attain it (6 m), are indicated by the dotted lines in the figure. However, there is no need to require the radiation level to be as low as 0.5 mrem/h since the induced activity from the target and other beam components will most likely limit the occupancy time and will likely be at the level around 5 mrem/h. Thus, a 5-m concrete wall would be adequate for shielding purpose. High-Z shielding can also be used near the target to reduce the amount of concrete. For example, Fe is roughly twice as effective for shielding high energy neutrons as concrete.

Low Energy Electron Dump

After the first bending magnet, the electrons that are captured and accelerated to about 230 MeV in the capture accelerator will be bent away from the positron beam trajectory and dumped. The average power of this electron beam is on the order of 10 kW, which necessitates a water-cooled beam dump. Two such dumps, made of a material such as copper, will be built on each side.

3.8.3 Radiation Hard Components

All components in the areas of high-radiation levels, particularly near the target and the low-energy electron dump, must be made of materials highly resistant to radiation. Particular consideration must be given to the the target chamber including vacuum and cooling water seals, the tapered-field and uniform-field solenoids, all electrical cabling, various magnets, and other diagnostic instrumentation immediately downstream of the first bending dipole.

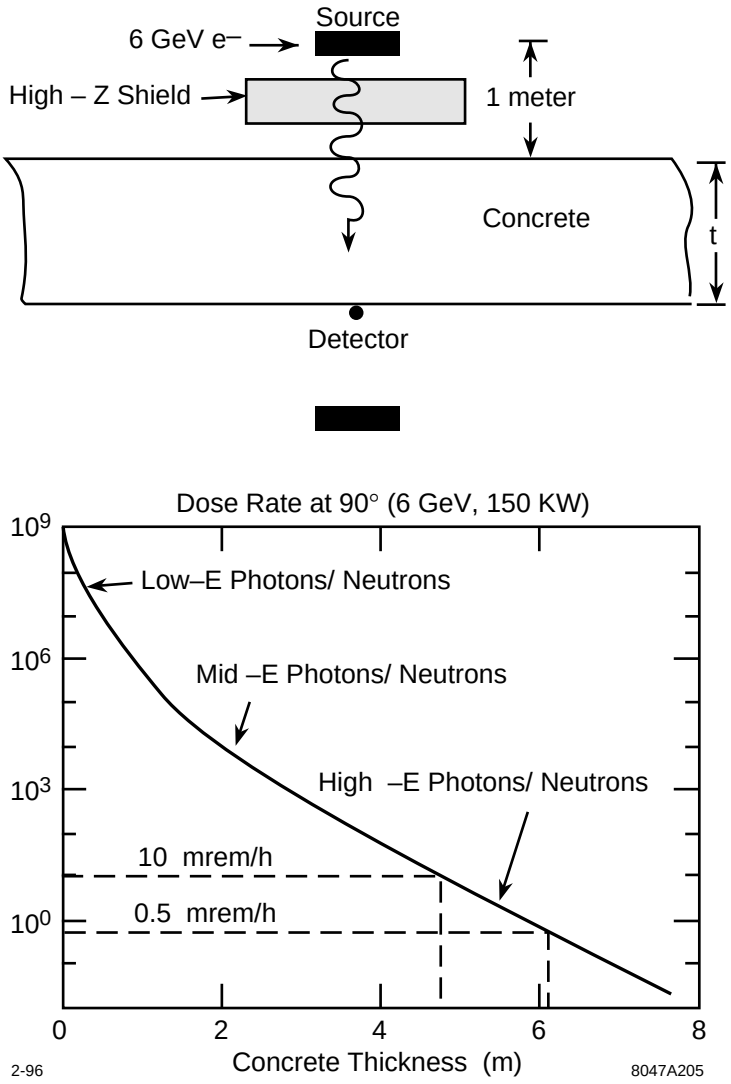

Figure 3-11. *Calculated radiation dose rate versus thickness of concrete shielding.*

3.9 Magnets

3.9.1 Solenoids

The tapered-field solenoid and the uniform-field solenoid are scaled-up versions of the SLC solenoids. Their inner radii need to be increased to approximately 11 cm and the total length to about 17 m to accommodate the four L-band accelerating sections, Their outer radii will also need to be increased accordingly to produce the required 1.2-T field at the front end which, over about 15–20 cm, tapers down to a field of 0.5 T and remains constant for the length of the uniform-field solenoid. The total power consumption of this solenoid will be on the order of 1.5 MW.

3.9.2 Quadrupoles

Two types of quadrupole magnets, one large aperture type that wraps around the L-band accelerating structures and the other regular type that wraps around regular beam pipes, will be used to construct the lattice for the 1.75-GeV L-band linac. Over 100 large-aperture quadrupoles are needed. They will have a pole-tip radius of approximately 11 cm, a length of 38 cm, and a pole-tip field of about 6 kg. Their power consumption is on the order of 15 kW each.

Another 50 or so smaller aperture quadrupoles will be used throughout the entire L-band linac, including approximately 20 for matching the positron beam from the solenoid-field region into the common L-band booster linac while maintaining an achromatic nature for this beam line section, and approximately another 20 for use in between accelerating sections and in the instrumentation section following the booster linac. This type of quadrupoles will have a pole-tip radius of 6.8 cm and a length of 36 cm, with a pole-tip field of about 6 kg.

3.9.3 Bending Dipoles

Six bending magnets, three before and three after the positron production and capture systems (Figure 3-10). are needed for directing the drive beam into either positron vault and directing the captured positron beam into the L-band booster linac. The latter three dipoles will bend the positron beam by 16°, and will have a 5.175-kg field, a 13.6-cm gap, and a length of 36 cm. The former three need to bend the 6.22-GeV electron beam by 10° each.

3.10 Diagnostics and Instrumentation

The bulk of instrumentation for the positron source, including the drive electron beam accelerator, is for routine optimization and diagnosis. While most of the instrumentation will be similar to what is used in the SLC, new instrumentation will be developed to diagnose the multibunch NLC beam. To maintain the beam quality, energy, energy spread, and bunch length will require continuous real-time monitoring before and after the target.

Many of these diagnostics and instrumentation will be used to address intensity jitter requirements. Measurements of intensity, energy, and position across the bunches of a train will need to be done to diagnose pulse-to-pulse variations in intensity out of the pre-damping ring. This is particularly important with beam intensity and energy since changes in these two attributes will lead directly to intensity fluctuations in the pre-damping ring.

Diagnostic	Bunch Train		Bunch Bundle	
	Range	Resolution	Range (per bunch)	Resolution (per bunch)
Toroid charge mon.	50–300$\times 10^{10} e^+$	$\pm$.2%	0.5–3.5$\times 10^{10} e^+$	$\pm$1%
Beam position mon.	0–2 cm	$\pm 20\mu$	0–2 cm	$\pm 20\mu$
Beam size mon.	$R = 0.5$–2 cm (edge)	$\pm$1%	$R = 0.5$–2 cm (edge)	$\pm$1%
Bunch length mon.	1–150 ns	$\pm$1 ns	10–100 ps	2 ps
Energy	250 MeV	$\pm$0.2%	250 MeV	$\pm$0.5%
ΔE at 250 MeV	$\sim$12%	$\pm$0.5%	$\sim$12%	$\pm$0.2%
Multi-strip mon.	Qualitative diagnostic for beam tuning			

Table 3-3. *Positron beam diagnostics and their specifications.*

3.10.1 Specifications

Beam diagnostic devices and their specifications for the drive electron beam have already been discussed in Chapter 2. Most of these diagnostics will also be used for the positron beam, but their specifications need to be modified slightly. Table 3-3 shows a list of the positron beam diagnostics and their specifications.

3.10.2 Beam Intensity

Bunch-to-bunch and pulse-to-pulse intensity stability will be measured after the drive beam electron gun, after bunching, and just upstream of the target. see Chapter 2 for more details.

The positron beam intensities will be measured immediately after the bending magnet which separates the electrons from the positrons, after the first L-band section in the booster linac, and at the end of the booster linac.

Bunch intensities will be sampled for beam-loading compensation feedback. High-bandwidth gap monitors appear feasible and development is in progress.

3.10.3 Beam Position

Position monitors, which measure the average bunch offset in a pulse train, will be placed in between every accelerator section near to or captured in any quadrupole magnet located there to monitor and, along with X/Y steering coils, correct and stabilize orbits via feedback loops. The centroid position of the bunches will also be important. High-bandwidth beam position monitors are feasible and development is being pursued but is expected to be expensive (see Chapter 15 for details). Placement of these monitors is lattice-dependent and in general will be used to diagnose and correct for wakefield and beam-loading problems. For the drive beam electrons, a set of these monitors to measure X, X', Y, Y' will be placed after the gun, after bunching, at the end of the S-band linac, and at two high-dispersion regions at 80 MeV and at the end of the linac (3.11 GeV for NLC-I and 6.22 GeV for NLC-II) for energy measurement.

For the positron beam, two sets will be used, one after the first bending magnet (after the electrons are separated), and the other between the L-band linac and the pre-damping ring.

3.10.4 Beam Size

The size of a small group of bunches, or perhaps of each bunch, will be determined with standard SLC-type wire scanners using high-bandwidth detectors (such as those under development in Japan). This will facilitate optical matching and emittance control tuning needed to minimize intensity jitter due to tails in the transverse distributions. For the drive beam electrons, a set to measure transverse phase space distribution will be located at the 80-MeV point, and another set at the end of the S-band linac before the double-bend achromats leading to the two positron production/capture systems. See Chapter 2 for more details. For the positron beam, two full sets will be installed, one after the first bending magnet, and the other at the end of the L-band linac before the pre-damping ring.

3.10.5 Beam Bunch Length

For the drive beam electrons, a bunch length monitor will be installed at the 80 MeV point after the beam is bunched (see Chapter 2). For positrons, three monitors will be used, one in each of the two double-bend achromats following the capture accelerators, and a third at the end of the L-band linac.

3.10.6 Energy

The energy of the drive electron beam will be monitored before the positron target, not only to facilitate its stabilization through feedback, but also to measure the effects of tuning methods and schemes for machine protection recovery. This can be done through high-bandwidth beam position monitors as described earlier.

The positron beam energy will be monitored at each available point to ensure the beam is centered in the aperture and to measure the effects of tuning methods and schemes for machine protection recovery. Monitors will be placed after the first few sections, and between the end of the linac and the pre-damping ring. The energy of the individual bunches will also be monitored at these locations. This should be done with high-bandwidth beam position monitors as previously mentioned. Wires could be used and they have the advantage of measuring energy spread as well, but are too slow for other uses.

3.10.7 Energy Spread

The energy spread of the drive electron beam will be monitored and maintained at a minimum just before the positron target . Wires with high-bandwidth detectors can be used for reliable quantitative measurements as in SLC.

The energy spread of the positron beam will be measured using multi-strip beam size monitors and wires with high-bandwidth detectors and maintained at a minimum. Measurements will be done at two dispersion locations, *i.e.*, in the double-bend achromat using foils as in the SLC, and in the linac to pre-damping ring transfer line.

3.10.8 RF Phase and Amplitude Monitoring

The shape of rf pulses will be sampled at frequent intervals to ensure phase and amplitude stability. Slow drifts due to diurnal effects, etc., will be compensated with feedback loops. Pulse-to-pulse sampling and correlation with beam changes can be used to determine severity. The SLC prototype has these features.

3.11 Feedback and Stability

Software-driven feedbacks with high-speed data acquisition, calculation, and device control were integral to the success of the SLC prototype (see Appendix D), and will be used in the NLC positron source to control orbit, energy, and beam-loading compensation.

A significant fraction of the drive beam power will be deposited into the first L-band section in the positron capture accelerator. The amount of power deposition in the first section depends on the machine repetition rate and on the bunch structure (*i.e.*, number of bunches per pulse) as well. In order to maintain rf phase and amplitude stability in the first section during periods of machine rate and bunch structure changes, the temperature of the structure must be stabilized by appropriately adjusting the cooling water temperature with special hardware and control software. Of course, thermal stability is equally important for the remaining three sections in the capture accelerator. Depending on the amount of power deposition into these sections, similar temperature control hardware and software may also be necessary for them.

An intensity feedback using the gun pulsar with the capability of changing individual pulses is desirable for long-term stability. A beam-loading compensation feedback will be needed to keep bunch intensity variations minimized as pulse train intensity may change.

3.11.1 Intensity Uniformity Specifications

The specifications on the pulse-to-pulse, or train-to-train, and bunch-to-bunch intensity jitters for the positron beam are 0.5% and 2%, respectively. Assuming there is no intensity jitter amplification (or growth) from the drive electron beam to the positron beam, these jitter specifications should also apply to the drive electron beam. A stable DC electron gun coupled with a jitter limiting aperture downstream is expected to provide an electron beam meeting these jitter specifications. Beam intensity diagnostics will have a .2% resolution for pulse intensity measurements and a 1% resolution for bunch or bunchlet intensity measurements.

3.11.2 Transverse Orbit Stability

Feedbacks for maintaining transverse orbit will be used throughout the entire system, but will be particularly important at critical points such as at the positron target or at the entrance to the pre-damping ring. The SLC prototype feedback is adequate and beam position monitors that measure the average bunch offset in a pulse train will be used.

3.11.3 Energy Control

Energy feedback loops will be needed in three places: before the target to control the energy of drive beam electrons; after the capture accelerator to control the energy of positrons to be launched into the linac; and in the linac-to-ring line before the entrance to the pre-damping ring.

3.12 Operations and Tuning Procedures

Operations and tuning procedures will be designed to grow toward higher levels of automation as in the SLC prototype. Initial procedures for commissioning and optimizing the positron source will lead to the development of algorithms and feedbacks for maintaining the positron source.

The systems in the NLC positron source are very similar to the SLC prototype and many SLC procedures will be transferable for use on the NLC. However, modifications and additions will be made to address issues involving the significantly higher beam power, multibunch operation, and machine protection schemes.

3.13 Control System Needs

3.13.1 Specification

The control system needs to monitor and control some of the devices on the time scale of the repetition rate of the machine, *i.e.,* 180 Hz for NLC-I or 120 Hz for NLC-II. This will require effective software-based feedbacks such as are used in the SLC prototype. On a slower time scale, the system must monitor and control a variety of devices to include rf amplitude and phase, magnet fields, and beam monitors of all types. These are just a few of the generic tools necessary for successful NLC operation.

3.13.2 Special Requirements

The positron source has two special requirements on the control system. (i) For the L-band capture accelerator, especially the first section, rf phase control for maintaining a constant positron yield will require thermal stability of the accelerating structures. During rate recovery from a machine protection rate change, thermal stabilization in these sections will require a pre-established feedforward control that promptly adjusts the temperature of the structure cooling water. (ii) The backup power system needs to be controlled in such a way that uninterrupted power is delivered to the various vacuum pumps of the positron target chamber in the event of a power outage.

3.14 Other Considerations

While the SLC positron source has met its design goal in terms of beam intensity and demonstrated good reliability over many years of operation, its success has been marred by the extensive and constant tuning effort required for operating the source and by excessive beam intensity jitter often experienced. The difficulty in operating the SLC source is known to be caused mainly by the lack of dedicated accelerators for both the drive beam and the positron beam which greatly limits the tuning flexibility. The excessive intensity jitter appears attributable to successively smaller apertures in the positron system starting from the capture accelerator to the damping ring. Accompanying a loss of beam intensity at each aperture, there is generally a concurrent growth in the intensity jitter. The accumulative effect leads to an increase in the positron intensity jitter, after being extracted out of the damping ring, by $\geq$75% over that of the drive beam.

Since the NLC positron source will have dedicated accelerators for the drive beam and the positron beam, its operational characteristics are expected to be improved significantly over its SLC counterpart. Also, since the smallest aperture in the NLC positron system by design is given by the capture accelerator immediately following the production target, minimal intensity losses are expected for the positron beam in the rest of the machine, including the L-band linac, the pre-damping, and the main damping ring. Judging from the SLC experience, one may expect that intensity jitter growth from the drive beam to the positron beam in NLC may be insignificant. Thus, producing a sufficiently stable drive beam may be the only critical task. This is, however, not to say that beam intensity jitter in the NLC positron source is a trivial issue. On the contrary, since intensity stability is such a critical issue to the success of the NLC, intensity jitter in the NLC positron source warrants critical design considerations.

3.15 Summary

The NLC positron source has a conventional design based on the SLC positron source and will be built with existing technology only. The significantly higher beam intensity for NLC is realized by the combined use of a larger drive electron beam on the target and an L-band positron accelerator. The former permits a quadratic increase in the pulse energy of the drive beam, while the latter permits the accelerating structure to have a minimum iris radius slightly more than twice as large as that of the SLC S-band structure, which translates into a $>$16-fold increase in the four-dimensional transverse phase space admittance. The source upgrade from NLC-I to NLC-II is straightforward, simply requiring an 80% increase in the drive beam size (area) and a doubling of the drive beam energy (from 3.11 GeV to 6.22 GeV). Both the NLC-I and NLC-II sources are conservatively designed to have large intensity safety margins—about a factor of 2.5 higher than the highest conceivable operating intensity at the interaction point—to insure against possible unforeseen beam losses.

The design employs a rotating positron target, intended for eliminating beam intensity modulations induced by target motion, with multi-stage differential vacuum pumping along the target drive shaft. Two identical, inter-switchable, positron production and capture systems will be built side by side to improve the source efficiency.

References

[Ecklund 1981] S. Ecklund, "Positron Target Material Tests", SLAC–CN–128 (1981).

[Helm 1962] R.H. Helm, 1962, "Adiabatic Approximation for Dynamics of a Particle in the Field of a Tapered Solenoid", SLAC–4 (1962).

[Kulikov 1991] A.V. Kulikov, S.D. Ecklund, and E.M. Reuter, 1991, "SLC Positron Source Pulsed Flux Concentrator", SLAC–PUB–5473 (1991), in Conference Record of the 1991 IEEE Particle Accelerator Conference, San Francisco, CA, 2005 (1991).

[Lynch 1989] H.L. Lynch, 1989, "ETRANS", SLAC Memorandum (1989).

[Nelson 1985] W. Nelson, H. Hirayama and D. Rogers, 1984, "The EGS4 Code System", SLAC–Report–265 (1985).

[SLC 1984] SLC, *SLC Design Handbook*, SLAC (1984).

[Thompson 1990] K.A. Thompson, and R.D. Ruth, 1990, "Controlling transverse multibunch instabilities in linacs of high energy linear colliders", SLAC–PUB–4801, in *Phys. Rev. D* **41**, 964 (1990).

Contributors

- S. Ecklund
- P. Emma
- G. Gross
- A. Kulikov
- R. Miller
- W. Nelson
- L. Rinolfi
- H. Tang
- K. Thompson
- J. Turner
- T. Umemoto
- V. Vylet
- D. Yeremian
- Z. Li